Int J Adv Manuf Technol (2016) 85:1261–1274
DOI 10.1007/s00170-015-8044-8

ORIGINAL ARTICLE

An improved soft abrasive flow finishing method based on fluid collision theory

Da-peng Tan[1,2] · **Shi-ming Ji**[1] · **You-zhi Fu**[1]

Received: 17 July 2015 / Accepted: 25 October 2015 / Published online: 4 November 2015

Abstract Soft abrasive flow (SAF) finishing has advantages in precise processing for the workpieces with tiny scale or irregular geometric surfaces. However, current SAF finishing methods have surface quality problem caused by uneven flow field profile. To resolve the problem, a novel double-inlet SAF finishing method is proposed based on the fluid collision theory. Taking two constrained processing apparatuses (single-inlet and double-inlet) as the objectives, in combination with the shear stress transport (SST) k-ω turbulence model, the fluid mechanic models for the two apparatuses are set up, and the preliminary abrasive flow field characteristics are acquired. Referring to the collision conservation principles, the profiles of dynamical pressure and turbulence intensity in double-inlet constrained passage are obtained. The simulated results show that the flow field distribution of single-inlet passage is in a steady state and non-uniform, a periodic oscillation phenomenon appears in double-inlet passage, and it can enhance the turbulence intensity and movement randomness of abrasive flow. The processing experiments show that the proposed SAF finishing method can make the roughness on parallel flowing direction less than 50 nm and can improve the finishing uniformity and efficiency.

✉ Da-peng Tan
tandapeng@zjut.edu.cn

[1] Key Laboratory of E&M, Ministry of Education and Zhejiang Province, Zhejiang University of Technology, Hangzhou 310014, China

[2] State Key Laboratory of Digital Manufacturing Equipment & Technology, Wuhan 430074, China

Keywords Precision processing · Soft abrasive flow (SAF) · Shear stress transport (SST) k-ω turbulence model · Double-inlet constrained passage · Fluid collision

1 Introduction

During the course of precise workpiece processing, the finishing procedure has the most intensive labor quantities and occupies more than 15 % of total processing cost [1, 2]. Considering the workpieces with simple or normal geometric structures, it can adopt traditional processing methods, such as precise turning, milling, or grinding. However, if a workpiece has complex structure, the traditional processing methods are hard to satisfy the technical requirements, while the loose abrasive particles with multiple cutting edges can resolve the matter [3–5].

The fluid-based processing is an effective method with loose abrasive particles, and it can break through the processing bottleneck of workpieces with complex structures. It is a flexible, precisely controlled, and thereby repeatable processing method of edge conditioning and surface enhancement in which the medium consisting of abrasive particles and fluid carrier is driven through or across the component for finishing [6]. Owing to the fluid flow characteristics, fluid-based processing can provide the desired, customized surface finishes on a broad range of simple as well as complex shaped or micro-size components [7]. Of course, concerning the randomness of fluid motion, the medium regulation is an important task to guarantee the material removal rate and surface quality.

According to the difference of operation mode, fluid-based processing can be divided into two categories: constrained and non-constrained. The first category contains the abrasive flow machining (AFM) [8], magnetorheological finishing (MRF)

[9], and hydrodynamic suspension polishing (HSP) [10]. The other one includes all kinds of jet processing methods, such as abrasive water jet (AWJ) [11] or magnetorheological jet polishing (MJP) [12]. With respect to the above methods, AFM requires to construct enclosed space in which the machined chips cannot be drained out and make the finished surface re-damaged. Moreover, MRF and MJP are limited by the magnetic components and hard to perform the precise processing for the complex workpieces. Therefore, with respect to the workpieces with tiny scale or irregular geometric shape surfaces, such as micro holes, helical grooves, thin slots, or large curvature passages, the above methods are hard to satisfy the expected technical requirements. For instance, there are four automobile part molds as shown in Fig. 1; the traditional processing methods would face serious challenges for all kinds of tiny scale or irregular geometric surfaces.

To resolve the matter, a novel no-tool finishing method, the so-called soft abrasive flow (SAF), is put forward [13, 14]. As shown in Fig. 2a, the traditional rotary grinding head cannot cope with the triangular slot. The SAF finishing method is composed of four fundamental components (shown in Fig. 2b), which makes a constrained tooling on the workpiece surface and constructs a constrained re-circulating flow passage. In the constrained passage, the loose abrasive particles and fluid medium mix into the abrasive flow with low viscosity and high velocity and can adapt the triangular slot as well as other geometric shape surfaces.

During the course of processing, the abrasive flow can pass through the constrained passage with high velocity and form the turbulent flow state with different vortices. Accordingly, the turbulent flow drives the abrasive particles to generate unordered motions and processing effects on the surface. Owing to the random particle motions, SAF finishing can obtain more uniform surface quality. Moreover, the chips can be drained out by the re-circulating flow passage and avoid the damage of finished surface.

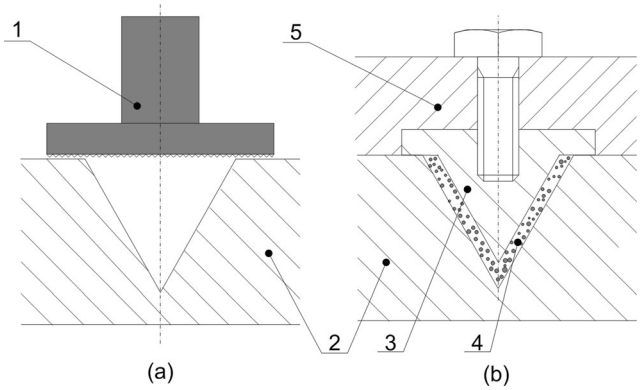

Fig. 2 SAF finishing working principle. **a** Traditional finishing method. **b** SAF finishing. *1* Traditional finishing tool (rotary grinding head). *2* Workpiece with tiny scale or irregular geometric surfaces. *3* Constrained tooling. *4* Constrained re-circulating flow passage. *5* Fixture

In view of the merits of the SAF finishing, it had been applied in some engineering areas, such as mold manufacturing and automobile accessories [13–16]. In 2010, Ji et al. adopted the discrete phase model (DPM) to set up a two-phase dynamic model oriented to SAF, and the simulation results showed that the abrasive flow machining process mainly appeared as translation of ablating location with the influence by granular pressure and as the variation of machining efficiency with the influence by near-wall particle velocity [17]. In 2012, Tan et al. presented a two-dimensional SAF dynamic model based on the topological structure transformation of level set method (LSM). The model could describe the movement of the particles in turbulent flow and reveal the dynamical variation regulars of phase surface of two-phase abrasive flow [18]. Li et al. proposed a SAF near-wall region

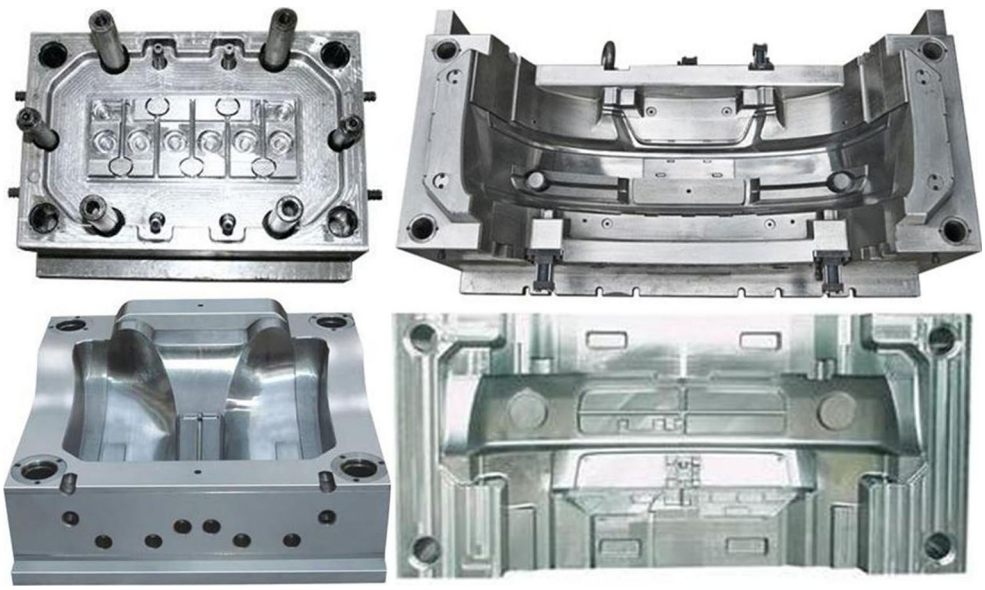

Fig. 1 Workpieces with tiny scale or irregular geometric surfaces

modeling method based on the Nikuradse's experimental principles. The variation trends of SAF turbulent parameters and flow passage pressure distribution with different inlet velocities were acquired by semi-implicit method for pressure-linked equation consistent algorithm. Experiment results showed that SAF could increase mold structural surface precision more than ten times, and the surface roughness in Ra value was less than 62 nm [19]. In 2014, Ji et al. put forward an ultrasound-enhanced SAF finishing method to increase the machining efficiency. The machining experiments showed that there are large numbers of bubbles that were growing and hitting on the wall continuously; the SAF coupled with ultrasound wave could reduce the machining time effectively [20].

Regarding the above studies of SAF, they all adopted the constrained flow passages with single-inlet. Because of the influences of the physical space restrictions and passage hydraulic diameter variations, the processed region of the workpiece surface takes on apparent non-uniformity. It is necessary to change the constrained tooling and working station to finish the total processing procedures, so the global working efficiency will be limited. To resolve the problem, we propose an improved double-inlet SAF finishing method. The method installs two inlets on the constrained passage with an angle and make two channels of fluid generate collision. The collision process can enhance the internal disturbance of abrasive flow in the passage, strengthen unordered movement and the turbulent intensity, and improve the profile uniformity of the flow field characteristics.

Apparently, the modeling and solution of fluid collision are the key scientific tasks of the paper. To address the above target, the corresponding research procedures are as follows. Firstly, based on the shear tress transport (SST) k-ω turbulence model and two-phase mixture model, the fluid mechanic models of the two kinds of constrained processing apparatuses (single-inlet and double-inlet) are set up, and the preliminary abrasive flow field characteristics are acquired. Then, according to the elliptic fluid collision theories, the fluid mechanic model is revised, and the profiles of dynamical pressure, turbulence intensity, and velocity in double-inlet passage are obtained. Finally, the double-inlet processing experiment devices are developed, and the experiments are performed to check the effectiveness of the proposed method.

It is well known that the issues of fluid collision are with big difficulties in the fluid mechanic area. The main scientific contribution of this paper is introducing the fluid collision theory into the fluid-based processing area and providing the modeling and solving methods. It not only can provide direct suggestions for the research works of the multi-channel fluid–solid contacting matters of constrained or non-constrained fluidic processing methods but can offer universal references to the engineering areas of large-scale hydraulic machinery design, chemical reactor internal state monitoring, and fluid–solid coupling resistance optimization.

This paper is organized as follows. In Section 2, the two-phase fluid mechanic model of SAF is set up based on SST k-ω turbulence model. In Section 3, the physical boundary conditions of the improved double-inlet constrained flow passage are described, and the fluid collision mechanic model is built. In Section 4, the numerical simulations for the flow field characteristics of the two constrained passages are performed, and the comparison analysis and discussions are given. In Section 5, a SAF finishing experimental platform is developed, and the experiments are finished. In Section 6, the conclusions are presented.

2 Fluid mechanic model of SAF

2.1 Fundamental control equations

According to the mechanical structure and working mode, we can find that the research objective of the paper is a two-phase incompressible fluid in a finite physical space and accords with the incompressible continuity equation and Navier–Stokes (N-S) equation [21–23]:

$$\frac{\partial u_i}{\partial x_i} = 0 \tag{1}$$

$$\rho\left(u_j \frac{\partial u_i}{\partial x_j} + \frac{\partial u_i}{\partial t}\right) = \rho K_i - \frac{\partial p}{\partial x_j} + \mu \frac{\partial^2 u_i}{\partial x_j \partial x_j} + \frac{\partial \tau}{\partial x_j} \tag{2}$$

where u_i and u_j (i, j=1, 2, 3) represent the components of velocity vector u on three coordinate directions, x_i and x_j represent the direction vector on three coordinate directions, p is the fluid pressure, ρ is the fluid density, μ is the kinetic viscosity, K_i is the gravity component, t is the time, and τ is the turbulent Reynolds stress:

$$\tau = -\rho\overline{u_i' u_j'} = \eta\left(\frac{\partial u_i}{\partial x_j} + \frac{\partial u_j}{\partial x_i}\right) \tag{3}$$

where u_i' and u_j' are the fluctuation velocity values, and η is the fluid turbulent viscosity.

Therefore, by solving the continuity equation and N-S equation, the profiles of pressure and velocity in the constrained flow passage can be obtained. Moreover, with respect to the SAF finishing, the abrasive flow is a kind of sparse two-phase flow, and the particle fraction is less than 30 %. In this hypothesis, SAF should have good fluidity and continuity, so the particle phase can be regarded as the pseudo-fluid for the fluid mechanic modeling.

2.2 SST *k*-*ω*-based fluid mechanic model

During the course of N-S equation solution, six Reynolds stress items will be generated and make the equation unclosed. Accordingly, the turbulent dynamic models should be combined to resolve the matter. Currently, there are some effective turbulent dynamic models, such as the standard *k*-*ε* model for high Reynolds number fluid, the renormalization group (RNG) *k*-*ε* model for large curvature passage, realizable *k*-*ε* model for high speed jet flow, and standard *k*-*ω* model for low Reynolds number fluid [24–26].

As shown in Fig. 2, SAF drives the abrasive particles through the constrained passage formed by the workpiece and tooling and uses the particle-wall collision process to remove materials. When the medium passes through the constrained passage, the processing action occurs at the fluid boundary layer of surface, i.e., the so-called near-wall region. It is well known that the study on near-wall flow field is a difficult point in fluid mechanic area. Traditional two-phase flow theories assume that the velocity of wall fluid is zero, and the second phase matter (solid) is commonly regarded as the pseudo-fluid [27, 28]. Because the abrasive flow in near-wall region is with lower Reynolds number, the turbulent models for high Reynolds number fluid are hard to obtain ideal computation accuracy.

As indicated above, the two-phase SAF has the following features: rotational flow, low viscosity, low Reynolds number, wall shear, and turbulence, while the SST *k*-*ω* turbulent model is suitable for the above features. Similar with other double-equation turbulent models, SST *k*-*ω* turbulent model contains a turbulent kinetic energy equation and a special dissipation equation [29, 30]:

$$\frac{D(\rho k)}{Dt} = \tau_{ij}\frac{\partial \boldsymbol{u}_i}{\partial \boldsymbol{x}_j} - \beta^*\rho k\omega + \frac{\partial}{\partial \boldsymbol{x}_j}\left(\Gamma_k \frac{\partial k}{\partial \boldsymbol{x}_j}\right) \tag{4}$$

$$\frac{D(\rho\omega)}{Dt} = \frac{\gamma}{\nu_t}\tau_{ij}\frac{\partial u_i}{\partial x_j} - \beta\rho\omega^2 + \frac{\partial}{\partial x_j}\left(\Gamma_\omega \frac{\partial \omega}{\partial x_j}\right) + 2\rho(1-F)\sigma_{\omega,2}\frac{1}{\omega}\frac{\partial k}{\partial x_j}\frac{\partial \omega}{\partial x_j} \tag{5}$$

where $\frac{D(\,)}{Dt}$ is the material derivative, $\tau_{ij}\frac{\partial \boldsymbol{u}_i}{\partial \boldsymbol{x}_j}$ is the partial derivative of the velocity vector, and τ_{ij} is the shear stress:

$$\tau_{ij} = \mu_t\left(\frac{\partial \boldsymbol{u}_i{}^i}{\partial \boldsymbol{x}_j} + \frac{\partial \boldsymbol{u}_j}{\partial \boldsymbol{x}_i} - \frac{2}{3}\frac{\partial \boldsymbol{u}_k}{\partial \boldsymbol{x}_k}\delta_{ij}\right) - \frac{2}{3}\rho k\delta_{ij} \tag{6}$$

In Eq. 6, $\boldsymbol{u}_k$ and $\boldsymbol{x}_k$ are the velocity component and direction vector on the third coordinate direction, respectively, and δ_{ij} is the Kronecker function:

$$\delta_{ij} = \begin{cases} 1 & i = j \\ 0 & i \neq j \end{cases} \tag{7}$$

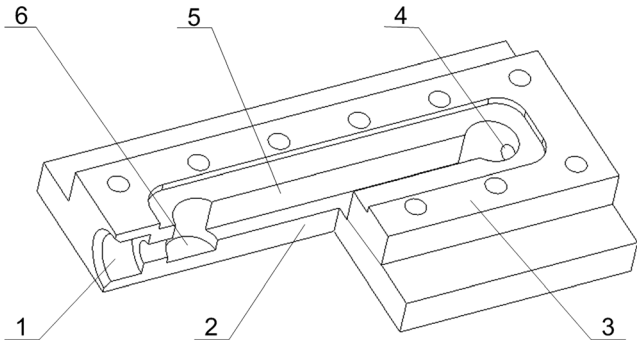

Fig. 3 Schematic illustration of the single-inlet SAF processing apparatus. *1* Passage inlet. *2* Foundation. *3* Constrained tooling. *4* Outlet. *5* Constrained passage. *6* Buffer hole

So, the partial derivative can be expressed as:

$$\tau_{ij}\frac{\partial \boldsymbol{u}_i}{\partial \boldsymbol{x}_j} = \mu_t\left[\left(\frac{\partial \boldsymbol{u}_i{}^i}{\partial \boldsymbol{x}_j} + \frac{\partial \boldsymbol{u}_j}{\partial \boldsymbol{x}_i}\right)^2 - \frac{2}{3}\left(\frac{\partial \boldsymbol{u}_k}{\partial \boldsymbol{x}_k}\right)^2\right] - \frac{2}{3}\rho k\frac{\partial \boldsymbol{u}_k}{\partial \boldsymbol{x}_k} \tag{8}$$

In Eqs. 4 and 5, Γ_k and Γ_ω are the effective diffusion items of k and ω; $\beta^*\rho k\omega$ and $\beta\rho\omega^2$ are the dissipation items of k and ω; and F is the switch function. The last item in Eq. 5 is the normal dissipation item for dissipation rate.

The effective diffusion equations are as follows:

$$\Gamma_\omega = \mu + \sigma_\omega\mu_t \tag{9}$$

$$\Gamma_k = \mu + \sigma_k\mu_t \tag{10}$$

$$\sigma_k = F\sigma_{k,1} + (1-F)\sigma_{k,2} \tag{11}$$

$$\sigma_\omega = F\sigma_{\omega,1} + (1-F)\sigma_{\omega,2} \tag{12}$$

where $\sigma_{k,1}$, $\sigma_{k,2}$, $\sigma_{\omega,1}$, and $\sigma_{\omega,2}$ are empirical constants. The switch function is

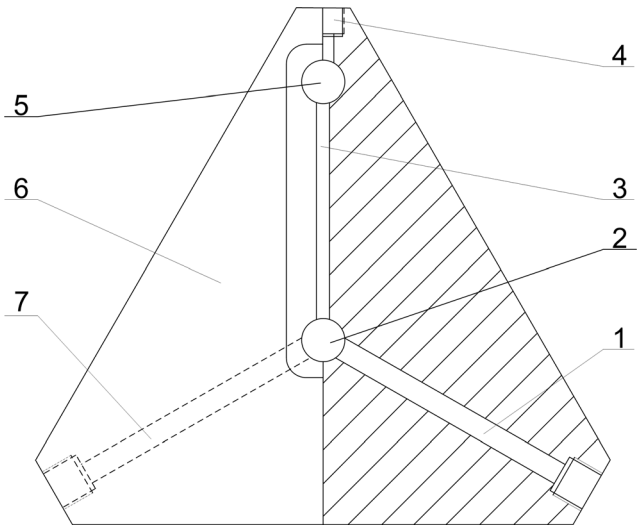

Fig. 4 Schematic illustration of the double-inlet SAF processing apparatus. *1* Passage inlet. *2* Input buffer hole. *3* Constrained passage. *4* Outlet. *5* Output buffer hole. *6* Constrained tooling. *7* Passage inlet

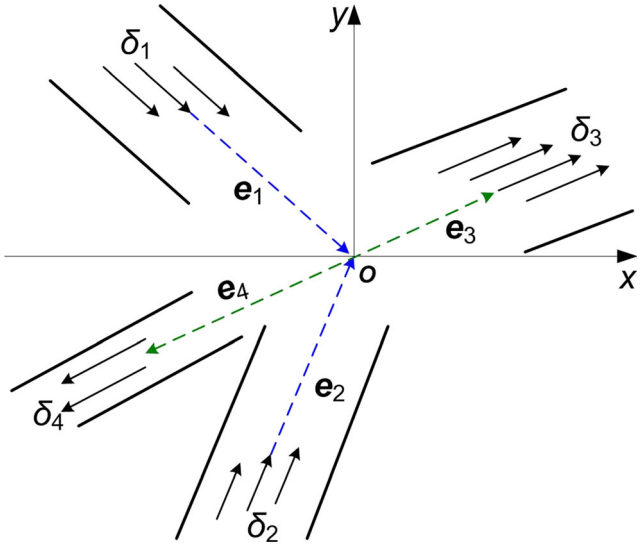

Fig. 5 Abridged view of fluid oblique collision

$$F = \tanh\left(\theta_1{}^4\right) \tag{13}$$

$$\theta = \min\left[C, \frac{4\sigma_{\omega,2}\rho k}{D^+ y^2}\right] \tag{14}$$

$$C = \max\left(\frac{\sqrt{k}}{0.09\omega y}, \frac{500\nu}{y^2\omega}\right) \tag{15}$$

$$D^+ = \max\left(\frac{2\rho\sigma_{\omega,2}}{\omega}\frac{\partial k}{\partial x_j}\frac{\partial \omega}{\partial x_j}, 10^{-20}\right) \tag{16}$$

In Eqs. 14 and 15, y is the distance of current target mass point to objective plane, and D^+ is the positive direction of normal dissipation item.

Apparently, the SST k-ω turbulent model, standard k-ω model, and standard k-ε model have tight internal relations. It is assumed that there are three correlation parameters, ϕ, ϕ_1, and ϕ_2, which represent the three models, respectively, and accord with the expression:

$$\phi = F\phi_1 + (1-F)\phi_2 \tag{17}$$

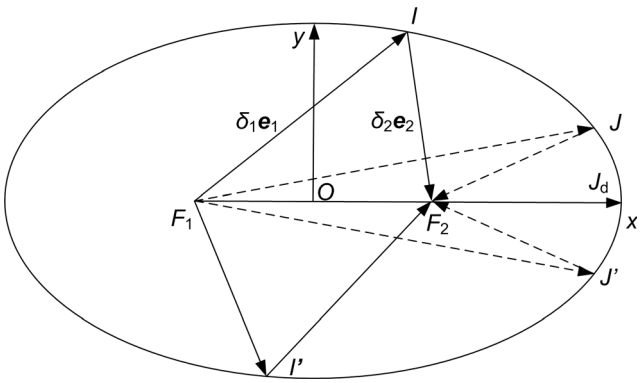

Fig. 6 Solution-elliptic model of fluid collision process

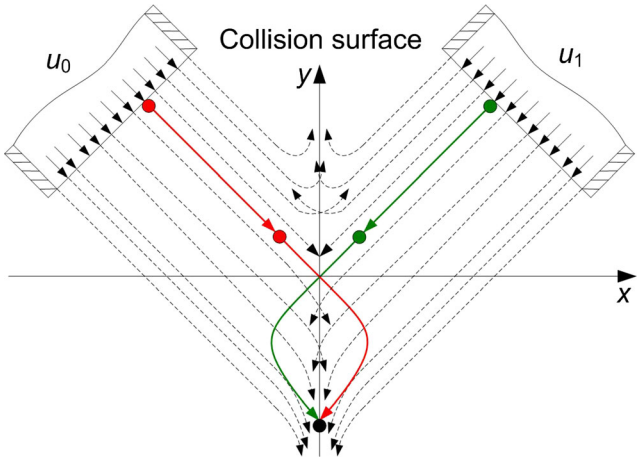

Fig. 7 Abridged view of abrasive collision process

If $F \to 0$, then $\phi = \phi_2$, and the SST k-ω turbulent model can transform into the standard k-ε model. The relevant empirical constants are as follows: $\sigma_{k,1}=0.85$, $\sigma_{\omega,1}=0.5$, $\sigma_{k,2}=1.0$, $\sigma_{\omega,2}=$

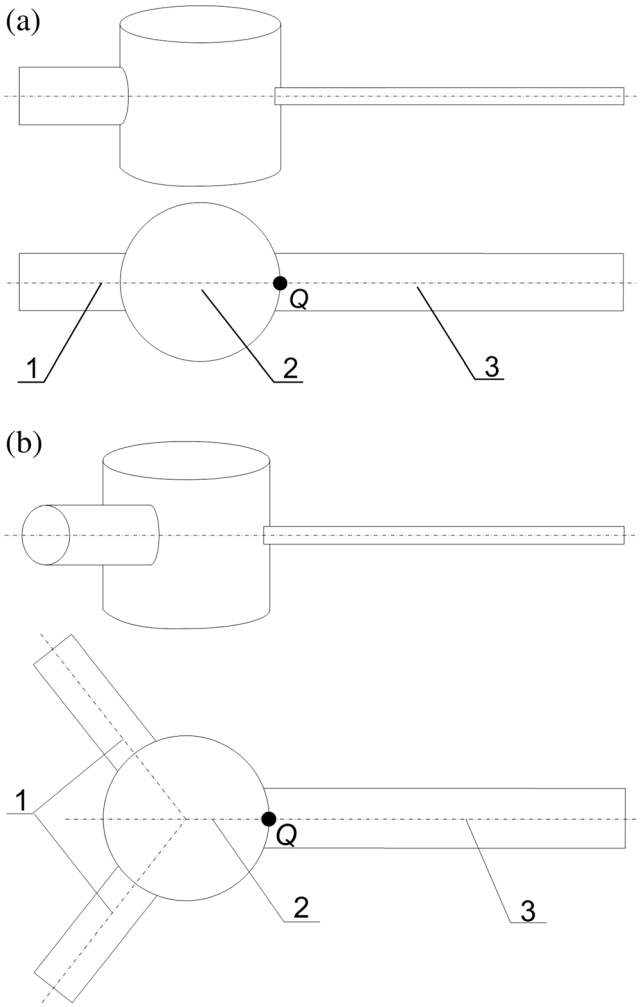

Fig. 8 Simplified geometric models of the two constrained processing apparatuses. **a** Single-inlet passage. **b** Double-inlet passage. *1* Inlet. *2* Buffer hole. *3* Constrained passage

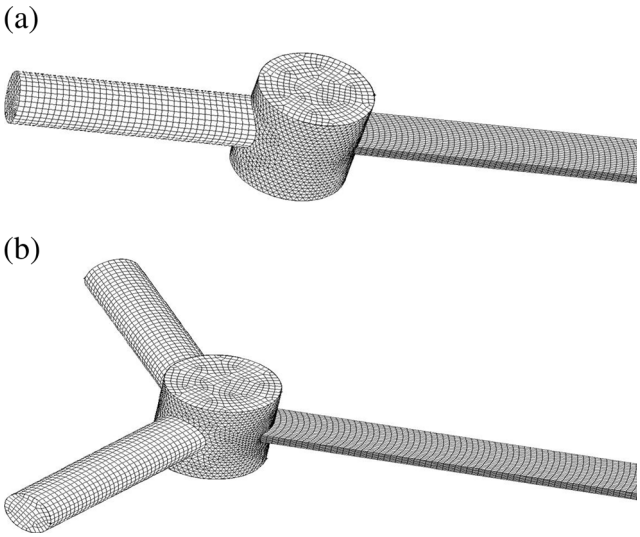

Fig. 9 Finite element models of the two constrained apparatuses. **a** Single-inlet passage. **b** Double-inlet passage; intensive meshing is performed on buffer hole and bottom surface of constrained passages

0.856, α_1=0.31, β^*=0.09, κ=0.41, $\beta_{i,1}$=0.075, $\beta_{i,2}$=0.0828, $\gamma_1 = \beta_{i,1}/\beta^* - \sigma_{\omega,1}\kappa^2/\sqrt{\beta^*}$, and $\gamma_2 = \beta_{i,2}/\beta^* - \sigma_{\omega,2}\kappa^2/\sqrt{\beta^*}$.

It is assumed that the vortex coefficient is

$$\nu_t = \frac{\alpha_1 k}{\max(\alpha_1\omega, \Omega F')} \tag{18}$$

$$F' = \tanh\left(\xi^2\right) \tag{19}$$

$$\xi = \max\left(\frac{2\sqrt{k}}{0.09\omega y}, \frac{500\nu}{y^2\omega}\right) \tag{20}$$

If $F \to 1$, then $\phi=\phi_1$, and the SST k-ω turbulent model will become the standard k-ω model. The relevant empirical constants are as follows: $\sigma_{k,1}$=0.5, $\sigma_{\omega,1}$=0.5, $\beta_{i,1}$=0.075, β^*=0.09, γ_1=5/9, and $\nu_t=k/\omega$.

Therefore, we can find that the above three models can transform each other during the transmission course from central turbulent region to near-wall region. It means that the models have adequate working flexibility oriented to different engineering computation instances and can obtain more accurate computation results. Moreover, the SST k-ω turbulent model is with mixing processing function that is designed for the near-wall region specially, so it can acquire reasonable flow field characteristics of SAF.

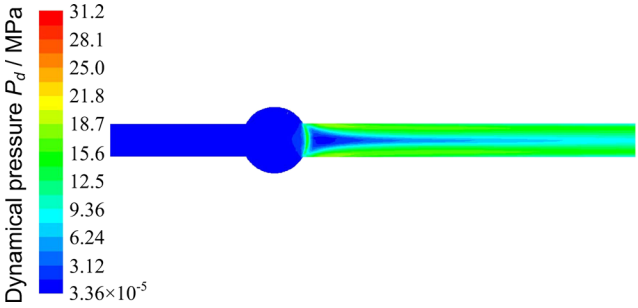

Fig. 10 Dynamical pressure profile cloud chart of single-inlet constrained apparatus

3 Double-inlet constrained passage and fluid collision model

3.1 The improved double-inlet processing apparatus

The single-inlet processing apparatus is shown in Fig. 3, where the SAF is exported from the pump and flows into the buffer hole by the passage inlet. Then, collision with the wall in buffer hole occurs and generates spiral backflow that can increase the disorder extent of abrasive particle movement. Subsequently, it enters the constrained passage and forms micro-force/quantity cutting effects by the particle-wall collision process.

As mentioned in Section 1, because of the influences of the physical space restrictions and passage hydraulic diameter variations, the single-inlet passage is hard to obtain ideal surface uniformity and high working efficiency of the integral finishing procedures. Therefore, we design a double-inlet constrained processing apparatus according to fluid collision principles, as shown in Fig. 4. It has two inlets with an angle, so the two channels of fluid will converge and collide in buffer hole and generate the required flow field with high disorder movement.

3.2 Fluid collision mechanic model

If the two inlets have the same parameters (pressure, velocity, geometric size, angle), the collision of two channels of fluid should be a symmetric collision. Supposing the angle of the two inlets is θ ($0°<\theta<180°$), the collision regular will be determined by the angle, i.e., the so-called oblique collision. Currently, the studies on fluid oblique collision are being the

Table 1 Physical parameters of two constrained processing apparatuses

	Inlet diameter/mm	Inlet velocity/(m s^{-1})	Reynolds number	Turbulent kinetic energy/(m^2 s^{-2})	Dissipation rate/s^{-1}
Single-inlet passage	10	40	8,695.65	6.37	6,580.22
Double-inlet passage	5	80	8,695.65	25.46	26,320.89

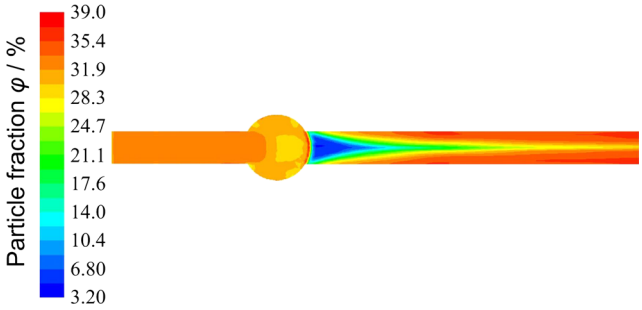

Fig. 11 Particle volume fraction cloud chart of single-inlet constrained apparatus

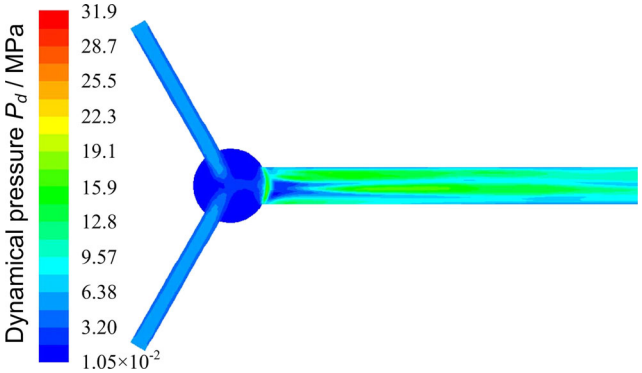

Fig. 13 Dynamical pressure profile cloud chart of double-inlet constrained apparatus

exploration stage that is caused by the uncertain steady solution. Therefore, the solution-elliptic model is a simple and effective research method for ideal fluid collision process [31–33].

Supposing the incompressible fluid pressure in which it is with infinite distance from the buffer hole is zero, the out-flow velocity along the streamline direction is equal to the in-flow velocity according to the mass and energy conservation equations. Apparently, the fluid oblique collision satisfies the above conversation equations. In this hypothesis, as shown in Fig. 5, it is assumed that the densities of two channels of in-flow are equal, the in-flow depths are δ_1 and δ_2, respectively, the in-flow velocities are equal, the in-flow direction vectors are $\boldsymbol{e}_1$ and $\boldsymbol{e}_2$, the out-flow depths are δ_3 and δ_4, and the out-flow direction vectors are $\boldsymbol{e}_3$ and $\boldsymbol{e}_4$, so the fluid collision conversation equations can be expressed as:

$$\begin{cases} \delta_1 + \delta_2 = \delta_3 + \delta_4 = 2a \\ \delta_1 e_1 + \delta_2 e_2 = \delta_3 e_3 + \delta_4 e_4 = 2ce_p \end{cases} \tag{21}$$

where a and c are characteristic constants, and $\boldsymbol{e}_\mathrm{p}$ is the vector sum of $\boldsymbol{e}_1$ and $\boldsymbol{e}_2$.

Supposing there are two in-flow vectors, $F_1I=\delta_1 e_1$, $IF_2=\delta_2 e_2$, the in-flow triangle expression is

$$\delta_1 e_1 + \delta_2 e_2 = 2c\mathbf{e}_\mathrm{p} \tag{22}$$

where I is the intersection point of $\delta_1\boldsymbol{e}_1$ and $\delta_2\boldsymbol{e}_2$, i.e., the theoretical collision point of two channels of abrasive flow in buffer hole. Then, taking $2c\boldsymbol{e}_\mathrm{p}$ as the baseline, and the out-flow triangle expression is

$$\delta_3 e_3 + \delta_4 e_4 = 2c\mathbf{e}_\mathrm{p} \tag{23}$$

where $F_1J=\delta_3 e_3$,$JF_2=\delta_4 e_4$, J is the intersection point of two channels of asymmetric out-flow vectors, and J_d is the intersection point of two channels of symmetric out-flow vectors.

Apparently, the vertices of the in-/out-flow vector triangles are all on an elliptic, as shown in Fig. 6, where OJ_d is the major axis, and $OJ_\mathrm{d}=2a=\delta_1+\delta_2$; F_1 and F_2 are the focus points that are the two endpoints of in-flow vector sum $2c\boldsymbol{e}_\mathrm{p}$; F_1F_2 is the focal length $2c$, and it is the base line of the in-flow triangle; and the vertex J of out-flow vector triangle is the solution of the fluid collision process.

As mentioned above, the out-flow solution of symmetric oblique fluid collision is J_d on elliptic. In the ideal hypothesis, the inlet parameters of double-inlet constrained passage should be equal, but the manufacturing and locating errors make the above conditions hard to satisfy.

The turbulent abrasive flow is with high-frequency fluctuation, which can lead to flow field variation of two channels of abrasive flow and make the out-flow intersection point oscillate around the theoretical solution. The oscillation will make the two channels of abrasive flow interpenetrate each other and increase the pulse pressure and movement randomness of particles, as shown in Fig. 7.

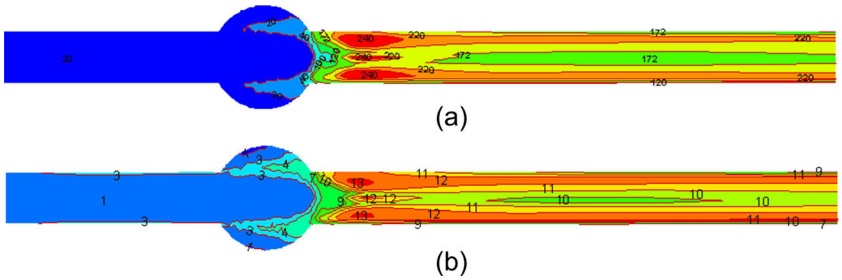

Fig. 12 Turbulence profile of single-inlet apparatus. **a** Turbulent kinetic energy. **b** Turbulent flow intensity

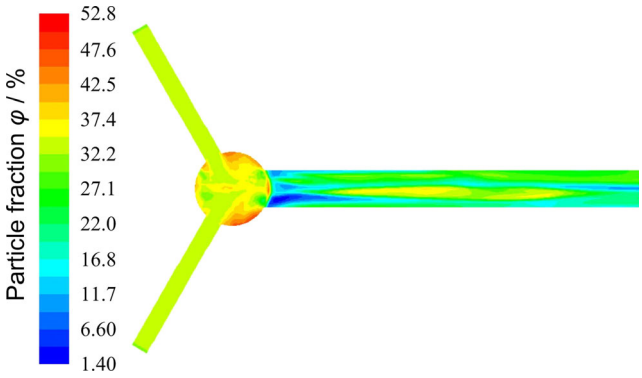

Fig. 14 Particle volume fraction cloud chart of double-inlet constrained apparatus

4 Numerical simulation and comparison analysis

4.1 Model simplification and mesh generation

In order to reduce the computation load of numerical modeling, some parts in geometric model should be simplified, as shown in Fig. 8. The simplified model only conserves the kernel components of SAF finishing apparatus, i.e., inlet, outlet, buffer hole, and constrained passage.

Mesh generation is the discrete processing of geometric model and influences the accuracy of numerical computation directly. Because the buffer hole and bottom surface of constrained passage easily appear stress concentration in the processing course, so they are meshed intensively by the hexahedral elements, as shown in Fig. 9.

4.2 Boundary conditions

In the processing procedures, the flow rate of pump requires to be kept constant and guarantees the processing stability; therefore, the pump flow can be regarded as a constant for numerical computation. For the double-inlet constrained processing apparatus, the pump flow is divided into two parts. If the head energy loss is neglected, so the flow rate of one inlet is half of that of the pump.

According to the above assumption, the boundary conditions are described as follows: the two-phase fluid model is the mixture model, the diameter of single-inlet passage is 10 mm, the diameter of double-inlet passage is 5 mm, the inlet condition is velocity inlet, the outlet condition is out-flow, the wall condition is solid wall, the first phase of abrasive flow is water, the second phase (solid particle) is SiC, the particle

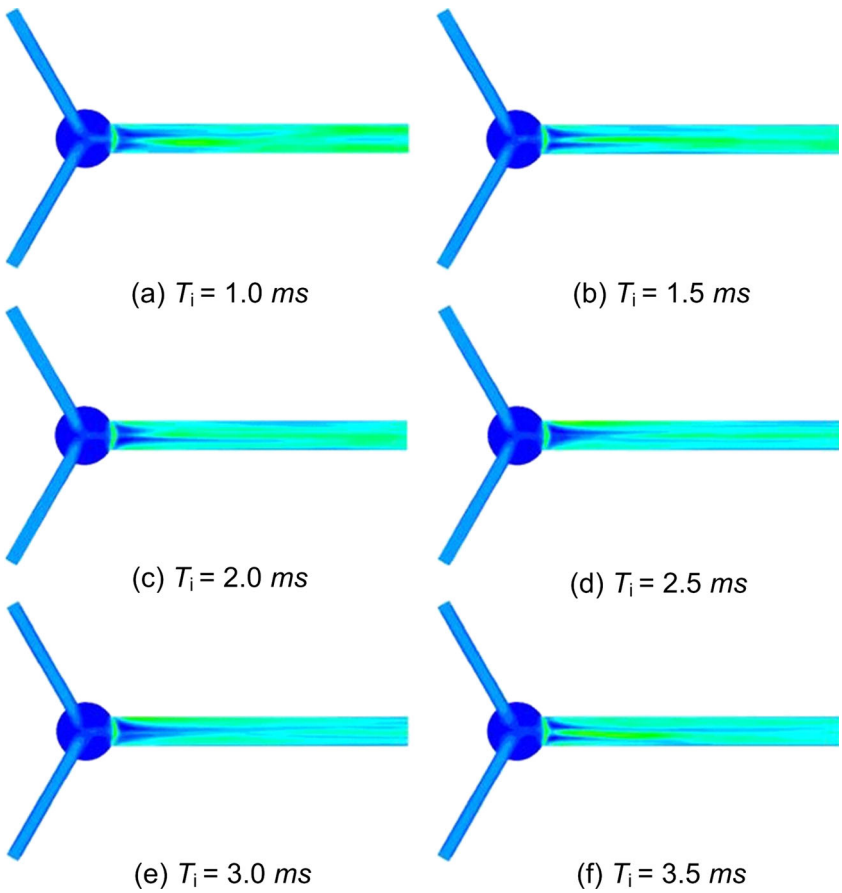

Fig. 15 Dynamical pressure profile cloud charts of double-inlet processing apparatus at different unsteady iteration time points

concentration is 20 %, and particle diameter is 5 μm, and the other numerical parameters are shown in Table 1.

As mentioned in Section 3, the fluid collision can cause the flow field oscillation in constrained passage, which is a classical unsteady flow process. Therefore, in order to observe the evolution mechanism of abrasive flow with the time variation, an unsteady solving method is selected to obtain flow field regulars, where the iteration step number is 400, and the time interval is 0.01 ms. Because the SAF is with higher velocity, a flow filed oscillation period should be less than in 2 ms. Accordingly, the iteration computation can contain at least two oscillation periods and satisfy the observation requirements of constrained passage flow field.

4.3 Numerical simulation of single-inlet processing apparatus

According to the Preston equation, it can be inferred that the dynamical pressure and velocity are the two key factors for material removal. The expression of dynamical pressure is

$$p_d = \frac{1}{2}\rho u_i^2 \tag{24}$$

From Eq. 24, we can find that dynamical pressure is relevant to density and velocity, so the profile regulars should be similar with that of velocity. Figure 10 is the pressure profile cloud chart of single-inlet constrained apparatus. In the buffer hole, the abrasive flow is with lower dynamical pressure, and the movement of abrasive particles is not intensive relatively. In the constrained passage, the dynamical pressure takes on the regular of two high lateral regions and low middle. At the inlet of constrained passage, there are two extreme values: the central region with minimum and the lateral region with maximum. Moreover, the global profile regulars of other time points in unsteady computation have not apparent variation.

The abrasive particle fraction is a key factor to finishing quality and efficiency. Figure 11 is the solid particle (SiC) volume fraction cloud chart of single-inlet constrained apparatus. In the buffer hole, there is higher and uneven particle fraction, which proves that the buffer hole can improve the intensity and randomness of particle movement. In the constrained passage, there is an apparent triangle region in which the particle fraction is lower, and the profile regular is similar with that of dynamical pressure. Moreover, the global particle fraction in the passage keeps unchanged by the variation of iteration time step.

As indicated above, turbulence is an important feature of SAF and with direct influence to the finishing effects. Turbulence is a symbol of internal energy of abrasive flow and can characterize the intensity of particle movement.

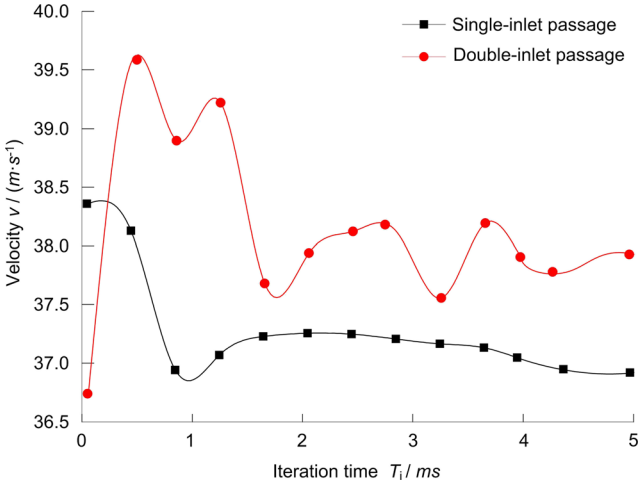

Fig. 16 Velocity variation curves of the two processing apparatuses

Figure 12 is the turbulence profile cloud chart of single-inlet constrained apparatus. From the figure, we can find that the profile regular of turbulent kinetic energy and turbulent intensity is consistent; after entering the buffer hole, the turbulent characteristics increase apparently; the bilateral regions of the constrained passage are with higher turbulent kinetic energy and intensity; and the maximum appears at the position near the inlet.

According to the above results, we can obtain the following regulars: the dynamical pressure, particle fraction, turbulent kinetic energy, and turbulent intensity of single-inlet apparatus are with fixed profiles and not relevant to the variation of time step in unsteady numerical computation; the profile characteristics of the above four parameters take on apparent non-uniformity that will cause negative influence to the processing quality and efficiency.

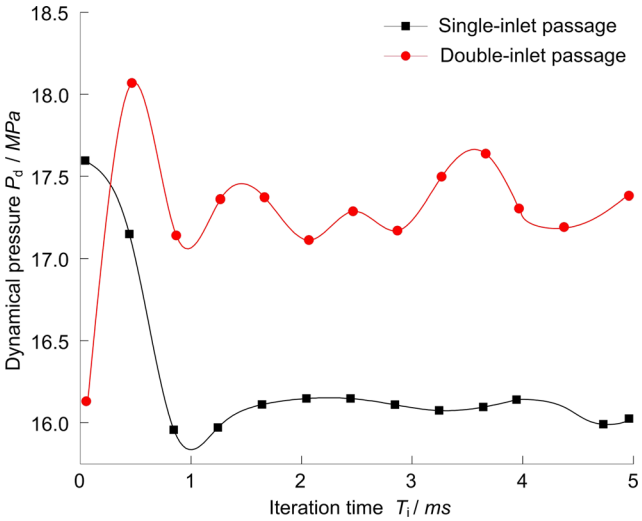

Fig. 17 Dynamical pressure variation curves of the two processing apparatuses

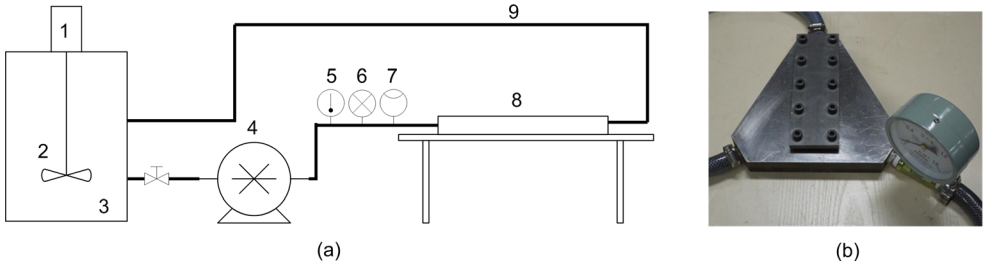

Fig. 18 Processing experimental platform. **a** Abridged view. **b** Physical entity of the double-inlet processing apparatus. *1* Motor. *2* Mixing blade. *3* Abrasive flow container. *4* Pump. *5* Thermometer. *6* Pressure meter. *7* Flow meter. *8* Processing apparatus. *9* Pipe

4.4 Numerical simulation of double-inlet processing apparatus

Figures 13 and 14 are the profile cloud charts of dynamical pressure and particle fraction in double-inlet apparatus, respectively. In the buffer hole, by the fluid convergence and collision process, two channels of abrasive flow interpenetrate and swap each other and enter constrained passage with higher turbulence intensity. In the constrained passage, the dynamical pressure and particle fraction break the stable triangle profiles of single-inlet passage and take on irregular profiles and better uniformities. Apparently, the above profile features are beneficial to improve the surface quality.

To observe the movement regulars of SAF in double-inlet processing apparatus, six iteration time points in unsteady computation are selected to analyze the variation of dynamical pressure, as shown in Fig. 15.

From the figures, we can find that the triangle low-pressure region in single-inlet processing apparatus is disturbed by the fluid collision and oscillates periodically around the medial axis of the constrained passage; there is a high-pressure region, which appears at the passage inlet firstly, moves to the passage outlet with the time variation, and disappears at the outlet finally. Accordingly, the above periodical pressure variation makes all the passage surfaces to have the same liquid–solid contacting conditions and improve the finishing uniformity and efficiency.

The inlet is a key position of the constrained passage and can characterize the flow field features of the passage. Taking the inlet medial point Q as the observation point (shown in Fig. 8), the corresponding velocity and dynamical pressure curves are shown in Figs 16 and 17, where the horizontal coordinate is the unsteady iteration time T_i, and the vertical coordinates are velocity v and dynamical pressure P_d, respectively. The initial influx velocity of single processing apparatus is 40 m/s, and the particles require to take 1.5 ms to arrive at Q. The initial velocity of double-inlet apparatus is 80 m/s, and the time flowing to point Q is 0.75 ms.

From the figures, we can obtain the following regulars: (1) Velocity and dynamical pressure in single-inlet apparatus enter the steady state on 1.5 ms, and the steady time of double-inlet is 1 ms. (2) In the transition process to steady state (0 ms$<T_i<$0.5 ms), the double-inlet is with lower velocity and pressure that are caused by the negative-pressure back flow of fluid collision; after converging of two channels of fluid, because they have higher initial influx velocities, the velocity and pressure increase rapidly and take on serious fluctuations. 3) The steady mean values of velocity and dynamical pressure of double-inlet apparatus are higher than that of single-inlet apparatus apparently. 4) The velocity and dynamical pressure at steady state are with limited fluctuations, and fluctuation amplitudes of double-inlet apparatus are larger than that of single-inlet apparatus.

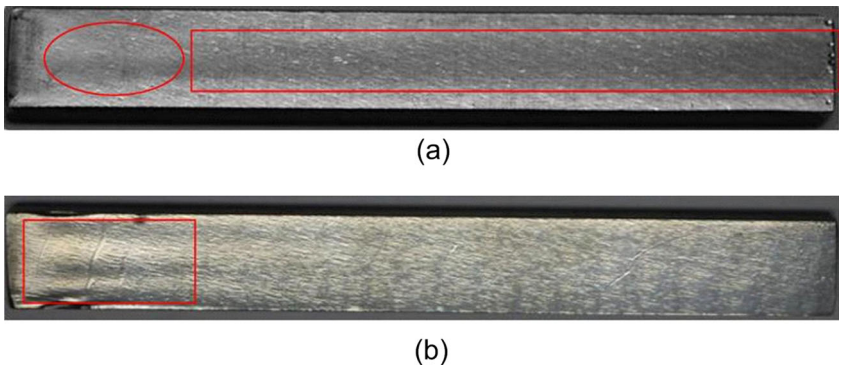

Fig. 19 Surface morphology comparison of the two processing apparatuses. **a** The processed surface by single-inlet apparatus. **b** The processed surface by double-inlet apparatus

5 Processing experiments and results analysis

5.1 Experimental platform and processing device

To check the effectiveness of the proposed method, a processing experimental platform is developed, as shown in Fig. 18.

5.2 Experimental result analysis

The experiments using the two processing apparatuses are performed, and the surface morphologies after 10-h processing are shown in Fig. 19. In Fig. 19a, there are no apparent material removal phenomena in the elliptic region; the rectangle region is with uniform processing effects and less material removal quantities; and the bilateral regions have higher lightness in which there are more apparent processing effects than other regions. Moreover, a photomicrographic apparatus with 500 amplification times is used to observe the micro morphology, and the results are shown in Fig. 20. In the central region, the original processing traces still exist, while the lateral region is with better surface quality. The above results prove that the single-inlet apparatus can cause apparent non-uniformity on surface quality and accord with the numerical simulation regulars in Section 4.3. In Fig. 19a, there are two etch pits in the rectangle region, which accords with numerical results in Section 4.4. In the other regions, apparent and even processing effects appear, and it can be inferred that the double-inlet processing method can resolve the non-uniformity problem of single-inlet method.

Figure 21 is the workpiece surface after 35-h processing by the double-inlet processing apparatus. From the figure, we can find that the processed surface can reach mirror level, which can reflect clear image, and has better uniformity.

In order to observe the processing effects of the parallel flowing direction and vertical flowing direction and analyze the surface roughness distribution regulars of the double-inlet processing method, the 16 observation points are selected, as shown in Fig. 22.

Figures 23 and 24 are the surface roughness curves of the processed surfaces after 40-h processing. On the vertical flowing direction, the average roughness processed by the single-inlet method can reach less than 0.4 μm, but the vertical 1 point has no apparent finishing effects, which is caused by the triangle region with lower dynamical pressure and particle fraction (shown in Figs. 10 and 11). Moreover, the roughness curves of other three observation points take on dispersion phenomena, which prove that the processing uniformity of single-inlet method requires to be improved. The average roughness processed by the double-inlet method is less than 0.2 μm, and curves of four observation points take on higher convergence, especially for the first one. Moreover, the double-inlet method only requires 15 h to reach the roughness level of single-inlet after 40-h processing, which prove that the double-inlet method can improve the processing efficiency apparently.

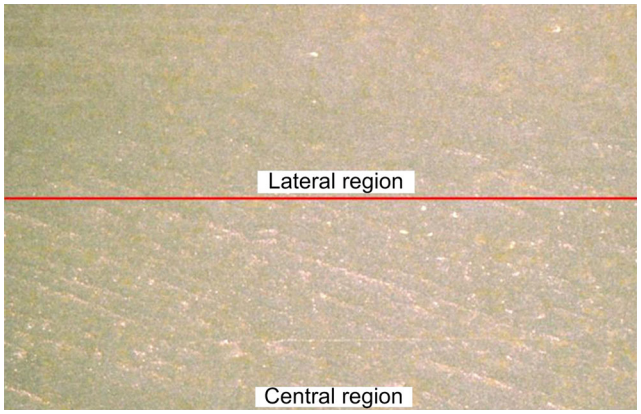

Fig. 20 The workpiece surface morphology using the single-inlet processing apparatus (lens ×50)

On the parallel flowing direction, the roughness of workpiece surface bilateral points (A and C) processed by the single-inlet apparatus is in the interval of 0.3–0.4 μm. Similar with the vertical flowing direction, the points A1, B1, and C1 are with the worst processing effects that are caused by the triangle low-pressure region. The roughness of central region (B) is in the interval of 0.2–0.3 μm, and with dispersed distribution. The results prove that single-inlet method can obtain better roughness in central region of constrained passage, but the processing uniformity still needs to be improved. The average roughness of the three surface regions (A, B, and C) processed by the double-inlet apparatus is less than 0.05 μm, and the curves are with better convergence and descending rate compared with the single-inlet method.

From the results of Figs. 19, 20, 21, 22, and 24, we can find that the double-inlet processing method has better finishing uniformity, precision, and efficiency than the single-inlet processing method, which might be caused by the following fluid mechanic regulars: (1) When the two channels of abrasive flow converge in the buffer hole, the intensive fluid collision process can increase the motion energy of abrasive particles, disturb the particle aggregation phenomenon, and improve the profile uniformity of the abrasive flow field. (2) In the single-inlet processing apparatus, because there are no flow disturbing factors, the profile characteristics in the constrained

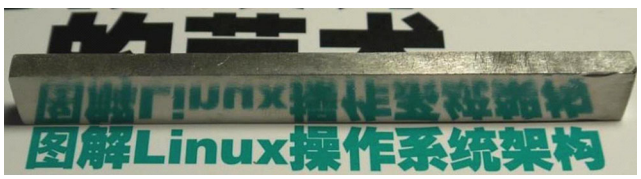

Fig. 21 The machined workpiece surface by the double-inlet processing apparatus

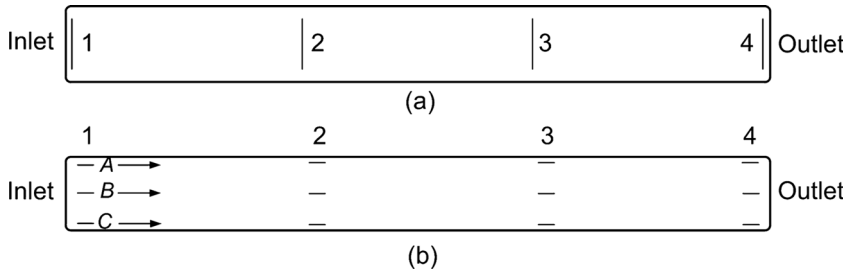

Fig. 22 The distribution of roughness measurement points. **a** Vertical flowing direction with four observation points. **b** Parallel flowing direction with twelve observation points

passage are steady. The double-inlet apparatuses introduce the interference flow, which cause the flow field profile oscillate, and make all the surface regions to have equal processing probability.

6 Conclusions

To address the processing non-uniformity problem of single-inlet SAF finishing, a novel double-inlet SAF finishing

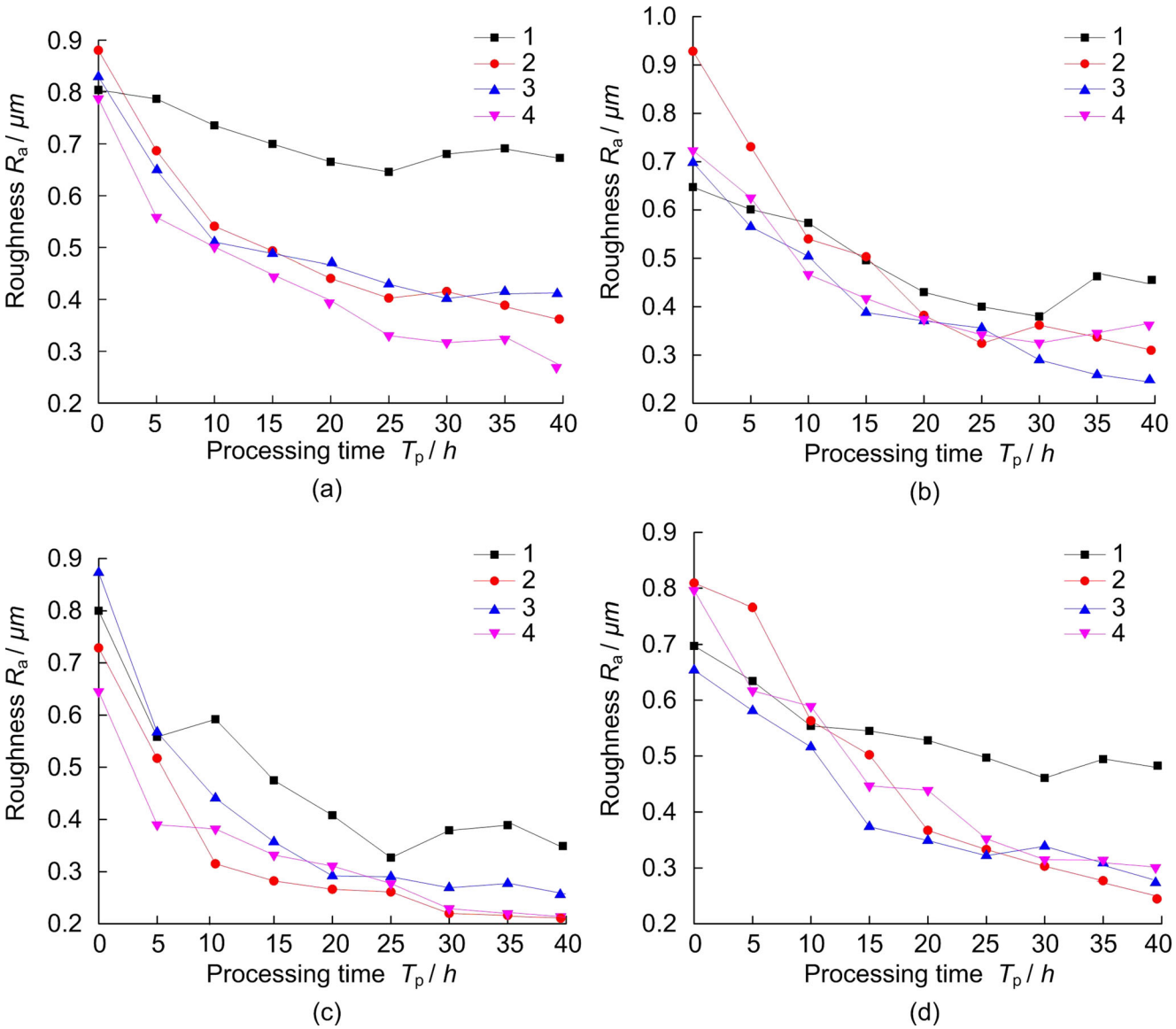

Fig. 23 Roughness variation curves of single-inlet processing method. **a** Vertical flowing direction. **b** Parallel flowing direction A. **c** Parallel flowing direction B. **d** Parallel flowing direction C

method is proposed based on the fluid collision theory. Considering the above research target, the corresponding theoretical modeling, and processing experiments performed, the main conclusions are as follows:

1. Based on the SST k-ω turbulence model and two-phase mixture model, the fluid mechanic models of the two processing apparatuses are built up. In combination with the fluid oblique collision conservation principles, the profiles of dynamical pressure and turbulence intensity in constrained passages are obtained.
2. In the single-inlet processing apparatus, owing to the variation of system hydraulic diameter and the limitation of constrained passage wall, there is a low-value region in the constrained passage, and the turbulent energy takes on decreasing tendency along the parallel flowing direction. If the boundary conditions are invariable, the flow field distribution of single-inlet passage is in steady state, which causes apparent non-uniformity on the processed surface.
3. In the double-inlet processing apparatus, the intensive collision of two channels of flow generates a periodic oscillation phenomenon on flow field profile in constrained passage. The oscillation can disturb the steady profile in single-inlet passage, enhance the turbulence intensity and disorderly movement of abrasive flow, and improve the processing uniformity and efficiency.
4. A SAF finishing experimental platform is developed, and the experiments have been performed. The experimental results accord with the numerical computation regulars

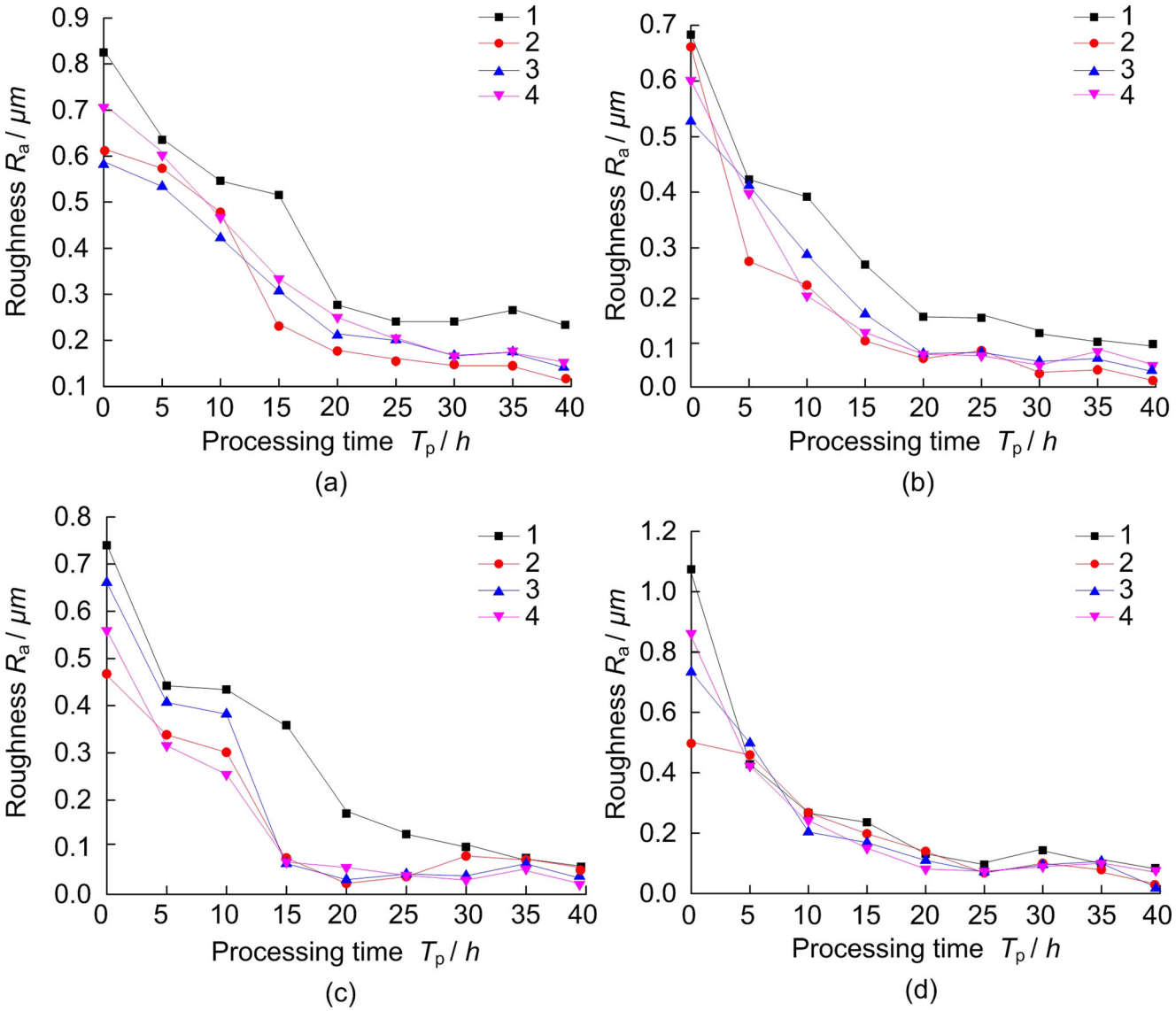

Fig. 24 Roughness variation curves of double-inlet processing method. **a** Vertical flowing direction. **b** Parallel flowing direction A. **c** Parallel flowing direction B. **d** Parallel flowing direction C

and prove that the proposed SAF finishing method can improve the uniformity, precision, and efficiency..

In general, the key scientific contribution of this paper is introducing the fluid collision theory into the fluid-based processing area and providing the modeling and solving methods. It not only can provide direct suggestions for the research works of multi-channel fluid–solid contacting matters of fluidic processing methods but can offer universal references to the engineering areas of hydraulic machineries or chemical equipment. The subsequent research works will be carried out around the facets of processing apparatus structure optimization and ultrasonic-based compound flow filed enhancing method.

Acknowledgments This work was supported in part by the Natural Science Foundation of China under Grant Nos. 51375446 and 51575494, the Zhejiang Provincial Foundation for Distinguished Young Scientists under Grant No. LR16E050001, the Commonweal Technology Project of Science and Technology Department of Zhejiang Province under Grant No. 2011R50011-05, the Visiting Scholar Foundation of the State Key Lab of Digital Manufacturing Equipment & Technology under Grant No. DMETKF2013006, and the Young and Middle-Aged Discipline Leader Climb Plan of Zhejiang Province under Grant No. PD2013020.

References

1. Zeng X, Ji SM, Jin MS, Tan DP, Ge JQ (2015) Research on dynamic characteristic of softness consolidation abrasives in machining process. Int J Adv Manuf Technol. doi:10.1007/s00170-015-7392-8
2. Nguyen T, Wang J, Li WY (2015) Process models for controlled-depth abrasive waterjet milling of amorphous glasses. Int J Adv Manuf Technol 77(5–8):1177–1189
3. Das M, Jain VK, Ghoshdastidar PS (2008) Analysis of magnetorheological abrasive flow finishing (MRAFF) process. Int J Adv Manuf Technol 38(5–6):613–621
4. Chen KY, Cheng KC (2014) A study of helical passageways applied to polygon holes in abrasive flow machining. Int J Adv Manuf Technol 74(5–8):781–790
5. Zeng X, Ji SM, Tan DP, Jin MS, Wen DH, Zhang L (2013) Softness consolidation abrasives material removal characteristic oriented to laser hardening surface. Int J Adv Manuf Technol 69(9–12):2323–2332
6. Rabani A, Marinescu I, Axinte D (2012) Acoustic emission energy transfer rate: a method for monitoring abrasive waterjet milling. Int J Mach Tool Manuf 61:80–89
7. Jang KI, Kim DY, Maeng S, Lee W, Han J, Seok J, Je TJ, Kang S, Min BK (2012) Deburring microparts using a magnetorheological fluid. Int J Mach Tool Manuf 53(1):170–175
8. Jain VK, Adsul SG (2000) Experimental investigations into abrasive flow machining (AFM). Int J Mach Tool Manuf 40(7):1003–1021
9. Das M, Jain VK, Ghoshdastidar PS (2012) Nanofinishing of flat workpieces using rotational-magnetorheological abrasive flow finishing (R-MRAFF) process. Int J Adv Manuf Technol 61(1–4):405–420
10. Joshi M, More S, Singh RK, Joshi SS, Balasubramaniam R, Suri VK (2012) Experimental characterization of hydrodynamic nanopolishing of flat steel plates. Precis Eng – J Int Soc Precis Eng Nanotechnol 36(3):424–434
11. Strnadel B, Hlavac LM, Gembalova L (2013) Effect of steel structure on the declination angle in AWJ cutting. Int J Mach Tool Manuf 64:12–19
12. Wang T, Cheng HB, Chen Y, Tam H (2014) Multiplex path for magnetorheological jet polishing with vertical impinging. Appl Optics 53(10):2012–2019
13. Ji SM, Tang B, Tan DP, Gong B, Yuan QL, Pan Y (2010) Structured surface softness abrasive flow precision finish machining and its abrasive flow dynamic numerical analysis. Chinese J Mech Eng 46(15):178–184
14. Ji SM, Xiao FQ, Tan DP (2010) A new ultraprecision machining method with softness abrasive flow based on discrete phase model. Adv Mater Res 97–101:3055–3059
15. Yuan QL, Ji SM, Tan DP, Zhang L (2011) Analytical method for softness abrasive flow field based on low Reynolds k-epsilon model. Adv Mater Res 188:230–235
16. Ji SM, Zhong JQ, Tan DP, Chi YW (2012) Research of distribution and dynamic characteristic of particle group in the structural flow passage. Key Eng Mater 499:271–276
17. Ji SM, Xiao FQ, Tan DP (2010) Analytical method for softness abrasive flow field based on discrete phase model. Sci China – Technol 53(10):2867–2877
18. Ji SM, Weng XX, Tan DP (2012) Analytical method of softness abrasive two-phase flow field based on 2D model of LSM. ACTA Phys Sin 61(1):010205
19. Li C, Ji SM, Tan DP (2012) Study on machinability and the wall region of solid–liquid two phase softness abrasive flow. Int J Adv Manuf Technol 61(9–12):975–987
20. Ji SM, Qiu Y, Cai YJ, Tan DP (2014) Research on mechanism of ultrasound enhancing and the experiment based on softness abrasive flow. Chinese J Mech Eng 50(7):84–93
21. Chen JL, Cai YW, Xu F, Hu HG, Ai QL (2014) Analysis and optimization of the fan-pad evaporative cooling system for greenhouse based on CFD. Adv Mech Eng 712740
22. Tan DP, Li PY, Ji YX, Wen DH, Li C (2013) SA-ANN-based slag carry-over detection method and the embedded WME platform. IEEE T Ind Electron 60(10):4702–4713
23. Li X, Kagawa T (2014) Theoretical and experimental study of factors affecting the suction force of a Bernoulli gripper. J Eng Mech 140(9):04014066
24. Chen JL, Xu F, Tan DP, Shen Z, Zhang LB, Ai QL (2015) A control method for agricultural greenhouses heating based on computational fluid dynamics and energy prediction model. Appl Energ 141:106–118
25. Tan DP, Zhang LB (2014) A WP-based nonlinear vibration sensing method for invisible liquid steel slag detection. Sensor Actuat B – Chem 202:1257–1269
26. Tan DP, Ji SM, Li PY, Pan XH (2010) Development of vibration style ladle slag detection method and the key technologies. Sci China – Technol 53(9):2378–2387
27. Zhao LS, Wang DH, Ye J (2005) Initial study of a theoretical near-wall turbulence model. J Aerospace Power 20(2):177–181
28. Tan DP, Li PY, Pan XH (2009) Application of improved HMM algorithm in slag detection system. J Iron Steel Res Int 16(1):1–6
29. Catalano P, Amato M (2003) An evaluation of RANS turbulence modeling for aerodynamic applications. Aerospace Sci Technol 7(7):493–509
30. Menter FR, Kuntz M, Langtry R (2003) Ten years of industrial experience with the SST turbulence model. Turbul Heat Mass Tran 4:625–632
31. Qin CS, Shi YN, Feng QJ (2007) The geometrical theory for the formation of asymmetric jet (I)—the geometrical close condition. Explo Shock Waves 27(6):493–500
32. Qin CS, Shi YN, Feng QJ (2007) The geometrical theory for the formation of asymmetric jet (II)—asymmetrical oblique collision. Explo Shock Waves 27(6):501–508
33. Li X, Horie M, Kagawa T (2014) Pressure-distribution methods for estimating lifting force of a swirl gripper. IEEE-ASME T Mechatron 19(2):707–718